Spring 2021

SILICON CARBIDE SYNTHESIS VIA ANION LOADED ACTIVATED CARBON

Auva Speiser

SILICON CARBIDE SYNTHESIS VIA ANION LOADED ACTIVATED CARBON

Spring 2021 Practicum Report

Auva Speiser

Montana Technological University

Butte Montana

Abstract

Silicon carbide (SiC) is a covalently bonded carbide ceramic with high hardness and resistance to wear and temperatures exceeding 1600 °C. Because of these properties, SiC is of interest to industries such as mining, aerospace, and high temperature electronic applications. However, because of the high amount of energy required to create this material, other more energy efficient methods are being researched.

In this study, SiC was synthesized from silicate anions adsorbed from solution onto activated carbon and carburized under a protective gas atmosphere. Initial runs were completed using 1 g of precursor material, in an inert gas atmosphere to determine run parameters and sample size adequate for characterization testing. Scale-up runs were completed using 5 g of precursor material, and both argon and hydrogen gas atmospheres were tested to determine the effect of a reducing gas atmosphere on synthesis yield. Material was characterized using X-ray diffraction with an internal standard of zinc oxide (ZnO) added to each sample in order to quantify SiC yields as a weight percent. Carburization behavior was modeled using response surface methodology to create statistical models that show the effect of time, temperature, and gas type on the SiC yield. Images of the carburized products were generated using scanning electron microscopy.

Silicon carbide whiskers were formed in the direction of the gas flow when temperatures in the furnace ranged from 1200 °C to 1400 °C with SiC yield increasing with increasing temperature and reaction time. The directional formation of SiC whiskers indicated that an intermediate gas phase was present during carburization, matching what has been concluded in previous work. Statistical models indicated that hydrogen gas did not significantly improve yield, which was contrary to existing literature. Fluctuations in H_2 flow rates may have affected results, indicating that gas flow rate may significantly affect SiC synthesis.

1. Background

1.1. Carbide Ceramics

Carbide ceramics are of interest to the automotive and aerospace engineering industries due to their high hardness, resistance to wear, and ability to withstand temperatures up to 1600 °C. These properties make carbide ceramics crucial materials in the production of the majority of cutting, milling, and mining tools [1]. All carbide ceramics are classified into three general categories: covalent, interstitial, and ionic carbides [2],[3]. Interstitial carbides such as tungsten carbide and molybdenum carbide form bonds that allow for smaller carbon atoms to fit in between the larger metal atoms that act as a host lattice [4]. Different stages of this process can be observed in the form of intermediate phases that are considered undesirable byproducts because they require additional energy to either continue or reverse the reaction. These intermediate phases are observable, so manipulation of key variables can achieve a maximum yield of the desired phase while minimizing the presence of intermediate phases [5]. Silicon carbide and boron carbide are known as ceramic carbides. Due to the covalent bonding structure of these carbides, ceramic carbides more rigidly hold onto shared electrons and do not form intermediate phases during synthesis unlike interstitial and ionic carbides, which transfer electrons more easily. These materials exhibit covalent properties due to silicon and boron having similar electronegativity and size to the carbon atom.

1.2. Silicon Carbide

Silicon carbide (SiC) has been utilized in a wide variety of applications and industries including aerospace optics, automobile break disks, lightning arresters, and high temp molten material vessels [6],[7]. SiC can perform in all these roles because it exhibits high thermal conductivity, high hardness, and chemical inertness shown in **Table 1**.

Table 1. Notable Properties of Silicon Carbide [8],[9].

Properties	Numerical value	Units
Density	3.1	g/cc
Dissociation/melting point	2,300	°C
Max use temperature	1650	° C
Hardness	2800	Kg/mm^2
Specific heat	0.67	J/g ° C
Thermal conductivity (at 20° C)	0.14	W/cm ° C

Silicon carbide was first synthesized by Edward G Acheson in 1891 when he was conducting research on the synthesis of artificial diamonds. The experiments he conducted involved mixing clay and metallurgical coke in a crucible and inputting energy into the crucible using a carbon arc-light furnace. When the mixture was removed from the furnace, bright green crystals were found attached to the electrode. Assuming the clay had imparted some aluminum into the complex, Acheson named the material carborundum after the aluminum mineral corundum. When Acheson conducted a hardness test on these green crystals, he found that the hardness was similar to diamond and applied for a US patent for the material.

Silicon carbide has been the subject of many studies and characterization attempts because of its diverse range of applications. Silicon and carbon are similar in size and the structure for silicon carbide results in each silicon and carbon atom being surrounded by four atoms of the other type. As a result, the SiC molecules can form into sheets on a single crystal plane. When another plane is stacked on top of the previous plane, a shift happens, and the molecules, in the form of tetrahedrons, become offset. The arrangement of molecules because of this shift is called a polymorph while the one-dimensional equivalent is called a polytype. Different polytypes of SiC happen when different molecular shifts occur [10]. Defects occur in the material when part of the material plane is misaligned from other molecules in the same plane [11]. However, the wide variety of polytypes that SiC can form makes synthesizing a specific polytype/orientation very difficult without forming a mixture of different crystal orientations. Crystal polytypes happen when a material is stable at different configurations within the crystal lattice.

The different arrangements the atoms can take to form SiC are shown in **Figure 1.** The numerical indicator describes the number of atoms in a row that follow the basic stacking sequence.

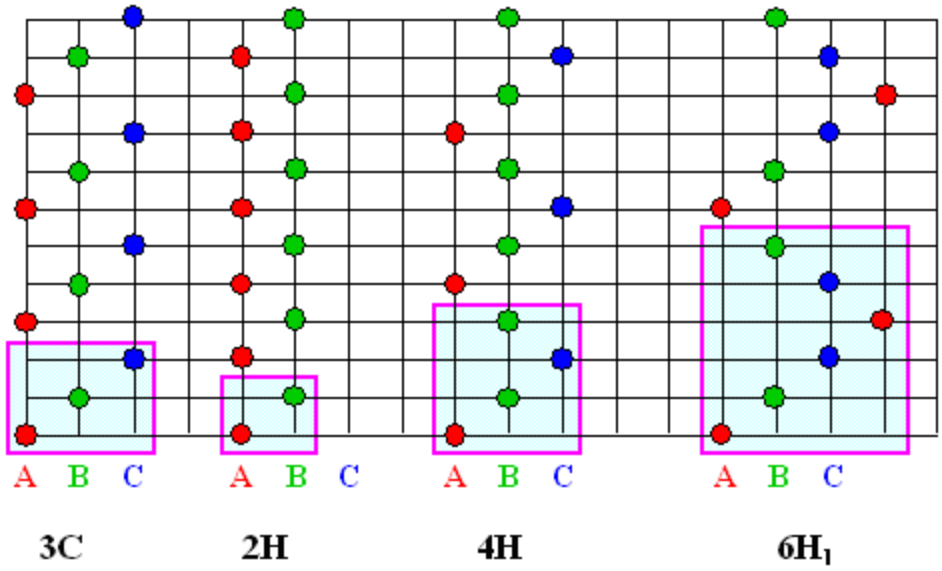

Figure 1. Alignment planes shown for SiC. The image indicates the types of arrangements that can be found in silicon carbide crystals with the numerical indicator stating how many atoms are placed in a set pattern before the pattern begins to repeat itself and the letter indicator stating the type of crystalline structure produced from this pattern [10].

For each polytype described, the numerical portion of the alphanumeric designation is the number of atoms in the stacking sequence. The letters following the stacking sequence indicator dictate the type of crystal structure the tetrahedrons in the stacking sequence produces; C being cubic, H being hexagonal and finally R being rhombohedral though it is not shown in the figure and rarely seen [12].

Due to the ease with which the material can form in different planar orientations, most SiC material is a mixture of different polytypes such as; β-silicon carbide which is cubic, or α-silicon carbide which can be hexagonal or rhombohedral [13]. The resulting material properties values can range widely due to the difference in each polytype's physical characteristics and natural defects. A majority amount of one

polytype can be produced using specialized processing methods; however, obtaining a large single crystal of one polytype is rare.

1.3. Kinetics of Silicon Carbide Formation

Silicon carbide kinetics and phase transition events are difficult to predict due to the lack of intermediate phases present when characterized. Phase transition events in the creation of silicon carbide are theorized to use different mechanisms than ionic ceramic carbides. Ionic ceramic carbides are created with other intermediate phases occurring in a process, and the system may not reach complete equilibrium at the time the process is halted so intermediate phases are produced alongside the final product. Silicon carbide lacking these intermediate materials is theorized to have an intermediate gas phase transition rather than a solid one [14], [15].

The equations involved in the formation of silicon carbide are as follows [16].

$$SiO_{2(aq)} + C_{(s)} \rightarrow SiO_{(g)} + CO_{(g)}$$

$$SiO_{2(aq)} + CO_{(g)} \rightarrow SiO_{(g)} + CO_{2(g)}$$

$$C_{(s)} + CO_{2(g)} \rightarrow 2CO_{(g)}$$

$$SiO_{(g)} + 2C_{(s)} \rightarrow SiC_{(s)} + CO_{(g)}$$

Because of the gas phase seen in the transition stages of the material, the finished product is the result of the mobile SiO gas phase interacting with the carbon precursor present.

1.4. Silicon Carbide Synthesis Methods

The manufacturing process for commercial abrasives is still much the same as the Acheson process. Silica sand and metallurgical coke are mixed and compacted around a carbon conductor to form SiC crystals [17]. The final product is then crushed to the desired size.

More advanced techniques and processes have been developed for SiC synthesis, for use in specialized applications. These specialized processes may be applied to produce a certain polytype of silicon carbide or to produce a specific shape of SiC complex such as wafers or fibers [18]. One of these methods is the reduction of SiO_2 in a graphite tube furnace with the presence of NaF or 3NaF·AlF3 to catalyze the reaction and reduce the activation energy and thermal energy required to produce SiC [19]. This method of creation was capable of producing β-silicon carbide whiskers in three different morphologies relating to different changes in the system and processing parameters. Silicon carbide whiskers have been observed to have planar faults perpendicular to the planar orientation and have been found to have a mixture of β and α polytypes [20],[21].

Another study used pitch as a carbon precursor and mixed it with a polymer gel containing silicon to ensure adequate contact between the carbon and silicon precursors. This paste was then heated up to 1400°C and silicon carbide whiskers were formed [22]. Other methods of creating silicon carbide utilized novel carbon precursors such as exfoliated graphite and woodchips [23]. Both materials were previously loaded with silica, via adsorption, and elevated to 1400 °C- 1425 °C under a reducing gas atmosphere of 25 % H_2 with the remaining atmosphere being made up of argon. In both cases, silicon carbide whiskers were observed ingrained into the carbon precursor [16].

1.5. Activated Carbon

Activated carbon (AC) has a history of uses in industrial fields such as water purification [24], pollution control[25], mining, and has also been used to treat poisonings in the medical field [26],[27]. These uses come from activated carbon's adsorption properties that are a result of the material's disordered microstructure[28]. In the 1770's, the adsorption of activated carbon was discovered by Scheele and used to adsorbed gases onto a charcoal surface. The next breakthrough involving activated carbon was in the 1790's when the material was used to aid in decolorization of water, making it viable for use in aqueous solutions. More than a decade later, the decolorization properties of activated carbon were being used to aid in color removal of various products, focusing mainly on sugar. In the 1800's, activated charcoal was demonstrated to prevent poisoning in animals and humans by adsorbing toxic chemicals, such as mercury bichloride, preventing absorption by the intestinal tract. Later, this technique would be applied in the creation of portable potable water from prepared carbon [27].

1.6. Properties and Microstructure of Activated Carbon

Activated carbon is a processed form of carbon with significant adsorption properties. Activated carbon is produced by carburizing organic material in an inert atmosphere. When volatile organics combust, they leave behind holes in the carbon material which make the material porous. The surface of activated carbon can be imagined as a defective and disorganized graphene layer. Graphene is typically carbon atoms connected in a hexagonal structure in sequence to form a single plane, with several of these planes stacked on top of one another, held together with Van der Waals forces. In the case of activated carbon, instead of forming a plane of material, the carbon atoms are attached in a random, three-dimensional structure that exerts significant Van der Waals forces on their surroundings, opening adjacent pores [28]. These openings size and shape are highly dependent on the source material when creating activated carbon leading to different operations needing varied carbon source material to maximize production [29].

Pores, like those seen in **Figure 2**., in the activated carbon structure are longer than they are wide; increasing the chance that a molecule will be affected by the Van der Waals forces before encountering the end of the pores. When this happens, molecules that are too large or not the right shape are unable to enter these pores., Products using activated carbon are carefully produced and engineered for specific applications, to take advantage of the fact that some molecules can be selected for by pore shape [29].

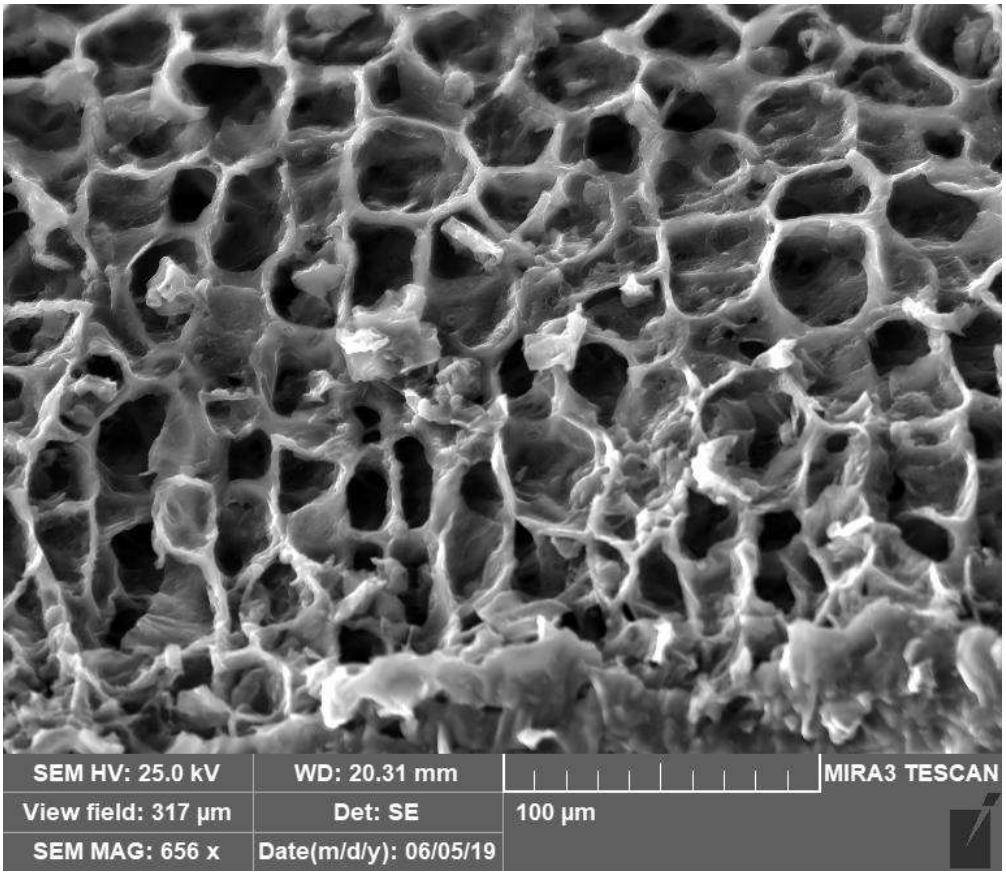

Figure 2. An example of pore size and shape in activated carbon created from coffee grounds [30].

Activated carbon adsorption capabilities can be used to adhere organic or inorganic material to its surface prior to a process unit. Impregnation of the activated carbon is done to increase effectiveness of existing activated carbon properties, provide a catalyst for material creation, or to be used an inert carrier material.

1.7. Objectives

The current work's goal was to reduce the energy required to create silicon carbide and better understand the variables contributing to its formation when created using activated carbon and an aqueous solution of sodium silicate. This was done following a novel method developed prior to this study [31] and statistical software was then used to analyze the data to observe optimal experimental ranges and determine statistical validity of the results.

2. Experimental

2.1. Adsorption of Material

Data obtained from prior scoping experiments were used in this study to determine the optimal adsorption procedure yielding the highest silicon to carbon ratio in precursor [5]. The previous study determined that a concentration of 21.734 g of sodium metasilicate per 100 mL of water produced a concentration of around 50,000 ppm Si. This solution was then mixed with 2.5 g of activated carbon and agitated at 400 RPM, on an IKA KS 130 Basic orbital shaker, for 2 h in plastic containers. The carbon was

retrieved though the use of vacuum filtration and subsequently dried before being measured out and loaded into the furnace. During scale-up experimentation, the scale of adsorption increased to 217.34 g of sodium metasilicate and 1000 mL of water to produce 25 g of precursor per batch. The adsorption scoping experiments determined that for each gram of carbon 0.27 g Si/g C of silicon was adsorbed.

2.2. Carburization

For carburization experiments, an MTI-1500x GSL tube furnace with a 2 in diameter alumina tube was used. For initial samples and synthesis runs, 1 g of precursor was measured and loaded into an alumina ceramic boat and put into the middle of the furnace hot zone. To safely carburize the samples and ensure that the equipment remained in good condition, the furnace temperature increased in stages to avoid thermal shock. Temperature increased from room temperature to 200 °C at 5 °C / min once at 200 °C, the furnace was held at this temperature for 20 min to ensure thorough heating of the tube and to remove any excess moisture. After 20 min, the temperature then increased to 600 °C at a rate of 10 °C/min and held for another 20 min. After this temperature hold, the furnace increased to the final carburization at a rate of 8 °C /min and held there for the duration of the experiment. Once the experimental procedure was completed, the furnace allowed to cool to 800 °C at a rate of 8 °C /min and from there allowed to cool naturally. Each carburization run was conducted under a purging inert argon (Ar) gas flow rate of 0.5 L/min. The Ar gas was present from when the furnace was started until the furnace was completely cooled to ensure carburization reactions were not disrupted by the presence of oxygen. Additionally, this slow cooling prevented harmful pressure drops due to increasing temperatures. Initial samples and scale-up experiments were conducted under a pure argon atmosphere for the duration of the experiment.

Scale-up runs that tested the effects of a reducing atmosphere were conducted using H_2. Reducing gas runs were conducted at temperatures of 1100 °C, 1200 °C, 1300 °C, or 1400 °C. H_2 gas was also set to 0.5 L/min using a MesaLabs DryCal Defender 530+ primary gas flow calibrator. In previous work a reducing gas atmosphere increased yield of interstitial [5] and covalent carbide synthesis [15],[14], compared to inert atmosphere. As a result, a reducing atmosphere was hypothesized to increase silicon carbide yield.

Initial silicon carbide synthesis experiments were run at temperatures of 1100 °C, 1200 °C, 1300 °C, and 1400 °C. Each sample was measured to be 1 g of precursor in an alumina ceramic boat and loaded into the tube furnace. Once the furnace was programed to the appropriate temperature and the argon flow was set to 0.5 L/min, and the samples were allowed to carburize for 4 h, 6 h, or 8 h.

In the scale-up runs, two alumina boats were used due to physical constraints inside the tube furnace limiting available work areas and requiring the boats to be placed in the direction of gas flow rather than at the same location in the furnace, both boats were put in the same space each time and in contact with each other in an attempt to eliminate variables. To better understand the kinetics, the sample boats were tested individually and only directly compared to other test runs of the same boat placement. Boat placement is shown in **Figure 3** for clarity.

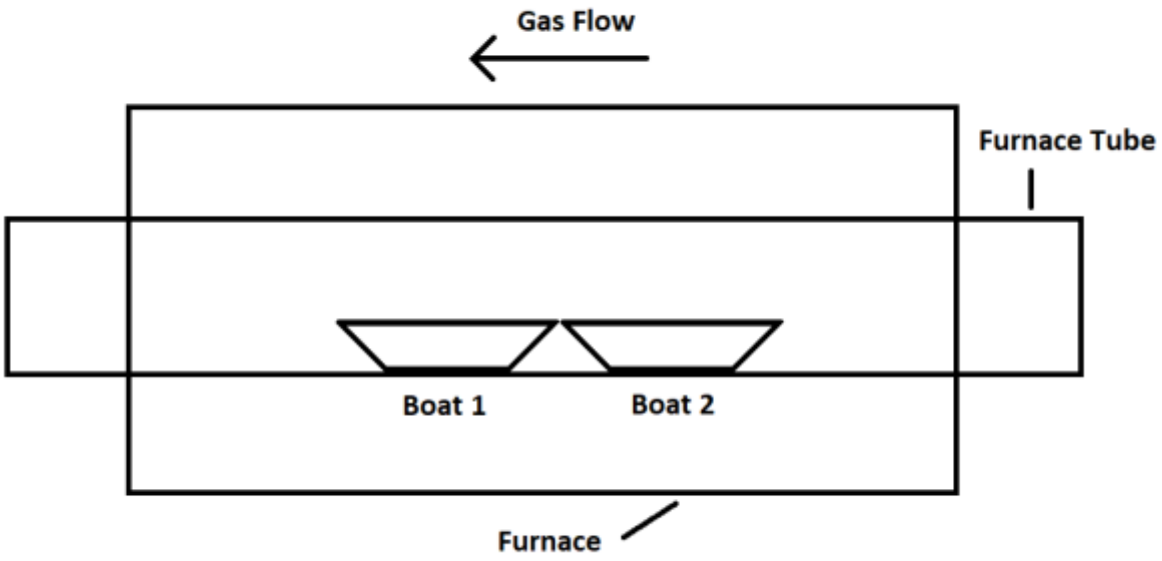

Figure 3. Furnace diagram depicting gas flow rate and sample boat placement.

Scaled up runs tested a temperature range of 1100 °C, 1250 °C, and 1400 °C at times of 4 h, 6 h and 8 h. For these runs 5 g of precursor was weighed out and split evenly into two ceramic and loaded into the furnace.

2.3. Characterization

2.3.1. Scanning Electron Microscope (SEM) Analysis

To acquire a visual image of the SiC samples, a cross section of the sample was taken and mounted on a sample stub and examined using Tescan Mira 3 scanning electron microscope. Normally, a carbon sample would be naturally visible to the SEM due to its ability to conduct a charge; however, the silicon carbide in the finished samples retained a charge and disrupted the characterization of the material. To properly characterize the samples, they were gold-coated to better observe the material and to reduce the charge accumulation and screen tearing issues introduced when a semi-conductive material is observed.

SEM analyses were not conducted on every sample due to a time constraint and the fluctuation of % yield calculations. The fluctuations are the cause of the heterogeneous nature of the samples and not enough sample was created each run to perform both XRD and SEM testing. Every SEM run required a separate furnace run as the SEM samples gold-plating would contaminate the results for XRD, and XRD sample prep would contaminate SEM samples.

2.3.2. X-Ray Diffraction (XRD) Analysis

X-ray diffraction (XRD) characterization was conducted using a Rigaku Ultima IV X-ray Diffractometer. The Rigaku used a Cu-Kα radiation at 40 kV and 40 mA for each sample. For initial samples, the sensors were calibrated to start at an angle of 10° from horizontal to read the reflected X-rays and a stop angle of 90°. It was determined from initial sample runs that starting from this angle produced a high amount

of noise due to the remaining amorphous activated carbon in the sample. As a result, subsequent scale-up runs were characterized starting from 20 degrees from horizontal to both reduce noise and provide a more accurate set of characterization data.

Silicon carbide does not reflect x-ray waves intensely, so an internal standard made of zinc oxide was added to all samples. The zinc oxide allowed for the comparison of silicon carbide peaks due to the zinc oxide having intense peaks and known peak locations to compare against. The software used for peak comparison was Jade (MDI Materials Data.), a software designed to interpret XRD Peaks into quantifiable data compared to known Material Peaks from the MDI Materials Database.

Each sample characterized using the Jade software had an additional 10% zinc oxide material added into it before being mixed. Because the zinc oxide was measured out, the variables obtained are in the form of a relative weight percentage.

2.4. Modeling

To ensure the statistical validity of planned scale-up runs, a response surface model was prepared using the DesignExpert 12 software suite, an experimental design and optimization software created by StatEase Inc. A response surface model utilizes user-specified design variables to aid in the design of statistically relevant models that test significant variables. For this work, temperature, time, and gas type were the primary variables tested, which DesignExpert 12 uses to generate design of experiments to assess the significance of these variables. These experiments are set in a random order to limit confirmation bias introduced when running similar runs consecutively.

Both initial run samples and scale-up run samples were analyzed through the DesignExpert 12 software to link design variables to XRD characterization results. The analysis then produces a synthesis model to interpolate likely results if runs were conducted in ranges between the tested variables. The model can undergo what is known as a transform. A transform is useful if the error in the plot produces a larger response than the predicted values. On the first iteration, no transform was selected to determine if a transform was necessary for further analysis of the data. If the first iteration of data indicated the need for a transform, then the analysis was ran again using the recommended transform. Once a transform was selected, fit statistics were evaluated to determine which model values to include based on how well the response values matched the predicted values and how relevant each model value was based on the fit statistics shown. Once model values were selected, the analysis of Variance (ANOVA) was ran to determine how well the model fits the data using diagnostic graphs such as the Box-Cox, Cook's distance, and predicted vs actual graphs. The produced graphs were frequently referenced to see if another transform would be applicable. After several iterations of analysis, a square root transform was deemed necessary for both scale-up and initial runs to best fit the model.

3. Results and Discussion

3.1. Scoping Experiments

Parameters were chosen in consideration to previous works [5] showing that silicon carbide forms at 1400°C, during a 20-hour run [31]. Initial run parameters, for this work, tested the silicon carbide synthesis efficiency in relation to time and temperature in the furnace. The times and temperatures selected are represented in **Table 2.** The data generally indicates that higher furnace temperatures coincide with higher amounts of silicon carbide formation.

Table 2. Initial run parameters and characterization results.

Sample name	Time (h)	Temperature (°C)	End Weight (g)	Silicon Carbide %
SiC_Ar_14C4	4	1400	0.4629	10.5%
SiC_Ar_13C4	4	1300	0.3757	12.3%
SiC_Ar_12C4	4	1200	0.5066	1.7%
SiC_Ar_11C4	4	1100	0.5604	1.3%
SiC_Ar_14C6	6	1400	0.3128	error
SiC_Ar_13C6	6	1300	0.3877	23.0%
SiC_Ar_12C6	6	1200	0.4545	error
SiC_Ar_11C6	6	1100	0.6167	1.0%
SiC_Ar_14C8	8	1400	0.4357	20.7%
SiC_Ar_13C8	8	1300	0.4572	11.7%
SiC_Ar_12C8	8	1200	0.3977	9.0%
SiC_Ar_11C8	8	1100	0.5976	0.3%

Each sample consisted of one gram of precursor that was dried in an oven for a minimum of 48h, however when entering the furnace, runs are conducted at high temperatures that dispel any unevaporated or bound water. The evaporating water and carburization reactions of silicon carbide synthesis cause many samples exiting the furnace to be less than half their original weight. The lack of sample to analyze from the first runs created difficulties for inputting data into the model. Two of the samples, SiC_Ar_14C6, and SiC_Ar_12C6, did not have enough sample to analyze in the XRD so the results returned as inconclusive and unreadable. These samples were omitted from the data input into the model for the scale-up runs. This lack of material was later accounted for in scale-up runs by using 5g of precursor to ensure sufficient product for characterization.

Figure 4. is an example of the XRD analysis using Jade software. On the left-hand side of the graph is a large anomaly that is produced by too many noise signals caused by the amorphous nature of activated carbon.

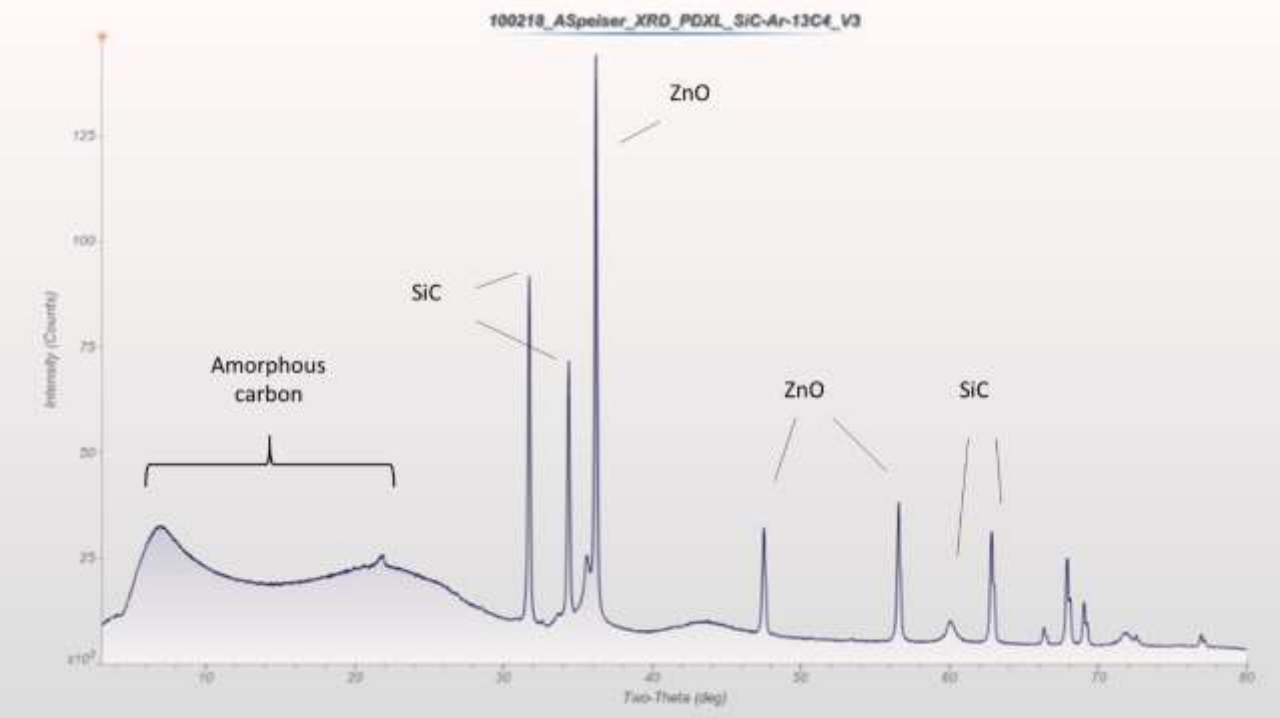

Figure 4. Graph showing the XRD results of an initial run sample, large abnormality and noise can be seen from 0-30 degrees, this abnormality is caused by the amorphous carbon contained in the sample material and disrupts further characterization measure.

Due to the large amount of noise present, peaks in the data were difficult for Jade to interpret. To counteract noise, subsequent XRD runs were performed three times for each sample at a start angle of 25 degrees. The readings could then be averaged to minimize sampling error.

The collected data was entered into DesignExpert 12 to determine significance in relation to the construction of a predictive model. **Table 3.** below are the ANOVA results when the above data is input into the model. When examining the ANOVA Design Expert software determined that the data entered was statistically valid. This validity can be deduced from the subsequent f-value of the model, a test to determine if the mean square of the model matches the mean square of the residuals, is larger than two. The p-values in the table detail what parts of the model have more significance to the outcome of the predicted silicon carbide synthesis values. p-values of less than 0.05 are considered significant values to the model while values greater than 0.10 do not hold as much significance to the model. From the model generated by the initial run data, temperature is a significant model value as it has a p-value of 0.0019, while time not as significant within the observed design space of between 4 h and 8 h according to the data with a p-value of 0.3505.

Table 3. ANOVA data results for initial silicon carbide synthesis runs.

Source	F-value	P-value
Model	8.26	0.0052
A-Time	1.00	0.3505
B-Temperature	23.42	0.0019

Table 4. indicates the fit statistics associated with data in **Table 3.** The fit statistics of the data, displayed as R^2, indicate the capability of the model to predict outcomes. R^2 and adjusted R^2 are measures of variance around the mean of the model indicating how far the data points fall from the predicted equation. Examining the predicted R^2 and adjusted R^2, both values have a difference of less than 0.2, indicating that the variance of model terms centered around the mean does not change drastically when adjusted for the number of terms in the model. Additionally, **Table 4.** contains the adequate precision term, which represents the signal to noise ratio, or difference in predicted values to actual values. When adequate precision measures greater than four it means the model can predict values that fall within the model range, and the model from the initial runs has a value of 8.8193.

Table 4. ANOVA fit statistics for silicon carbide synthesis initial runs.

Std. Dev.	0.8223	**R^2**	0.7772
Mean	2.65	**Adjusted R^2**	0.7136
Adeq Precision	8.8193	**Predicted R^2**	0.5646

Figure 5 (a) is the normal plot of residuals and indicates if the residuals of the data follow a normal distribution. **Figure 5 (b)** is the predicted vs actual graph where the variance of the data points is measured against the predicted responses, this allows for the detection of groups of data points that are not easily predicted by the model.

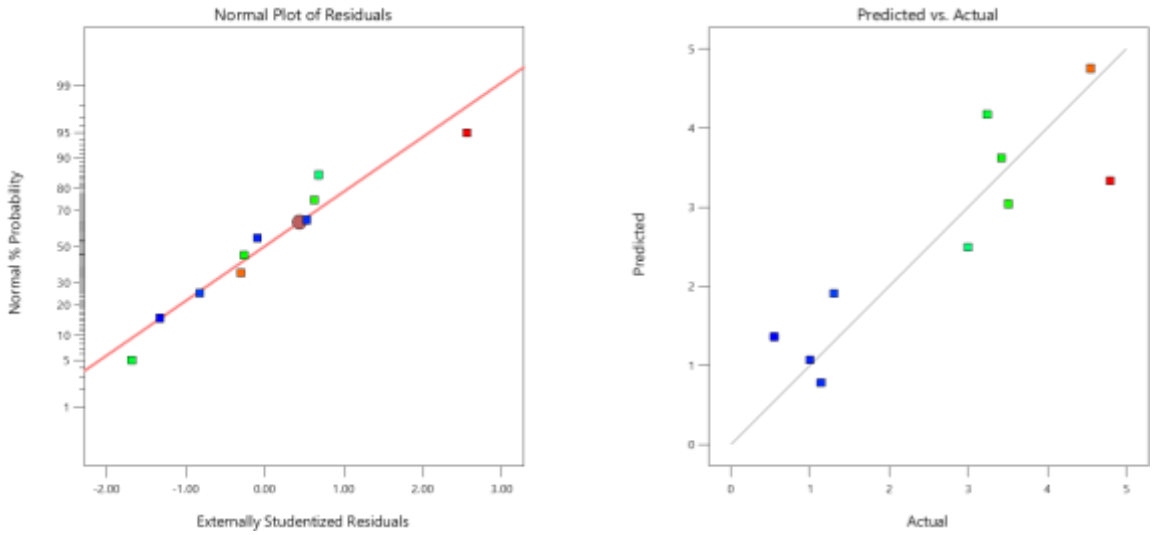

(a) **(b)**

Figure *5*. Normal plot of residuals (left) and predicted vs. actual (right) diagnostics graphs.

The graphs in **Figure 6**. are the Leverage vs. Run and Cook's distance diagnostics.

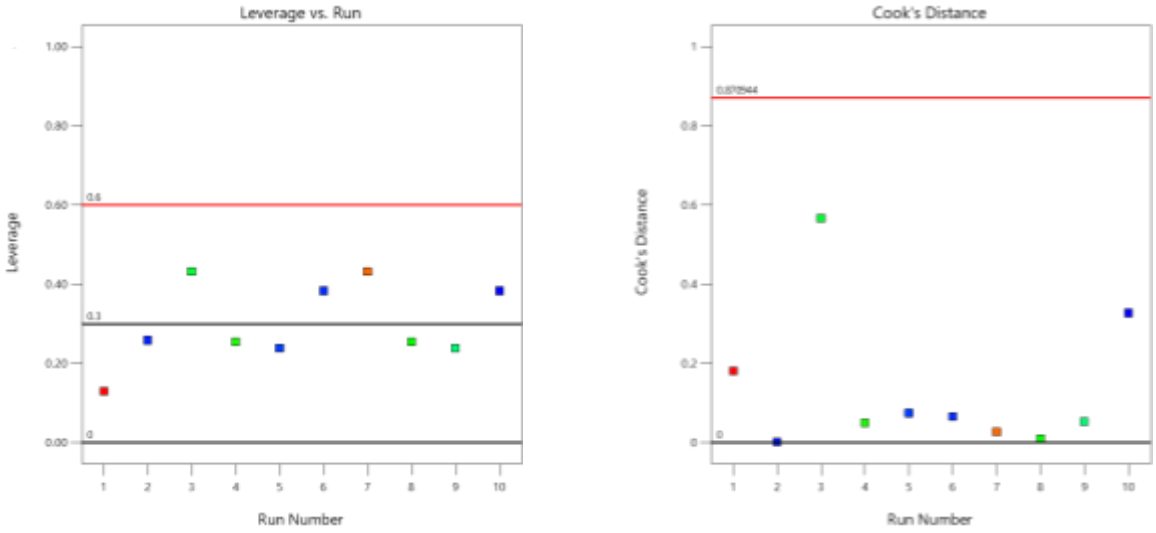

(a) **(b)**

Figure 6. (a) Leverage vs. Run (b) Cook's distance diagnostics graphs

The leverage vs. run graph shows how each data point influences the model and how well these runs fit the model. The data points don't exactly fit the model but fall into a cluster at an acceptable level below the red line shown in the graph. The image above and to the right displays the cook's distance, which indicates if outliers in the data are outside acceptable ranges. From the entered data, no outliers in the initial runs are indicated to fall outside acceptable limits.

The one factor interaction graph shown in **Figure 7** Shows how the interaction between silicon carbide synthesis is related to temperature at 4h. in the graph the black line shows times effect, and the dashed lines are the confidence intervals for the interaction. The red dots shown are the data points and how they measure against the model.

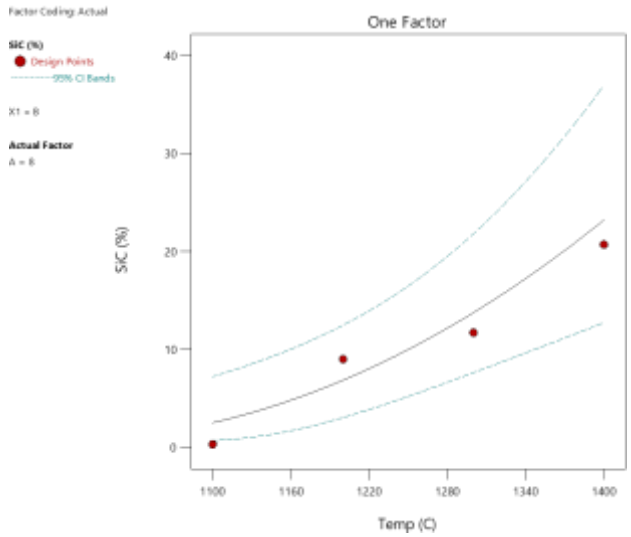

Figure 7. One factor interaction graph depicting the influence of temperature on silicon carbide formation under argon for 8 h for initial runs.

Figure 8. is the rendered response surface model of the initial runs and how this model would predict silicon carbide synthesis quantities when scaled up if performed under identical conditions.

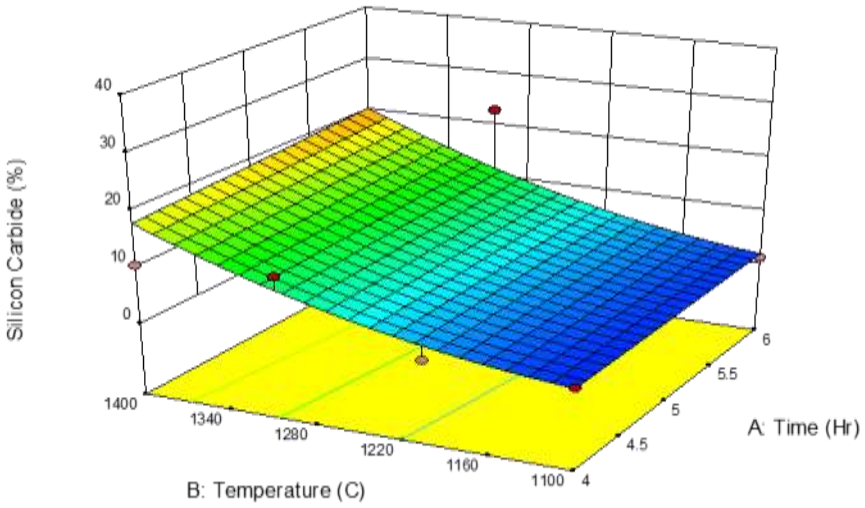

Figure 8. Silicon carbide synthesis historical data model.

The model shows that a higher SiC yield was obtained at a higher temperature showing an increase of 16%-20% yield from 1100 °C to 1400 °C. However, increasing time did not seem to have as drastic an effect on the yield as a maximum of 3% increase in yield was seen between 4h and 6h.

3.2. Scale-up Runs

Scale-up furnace runs were conducted using a response surface design matrix created from data gathered from the initial runs. Data captured from these runs would better represent characterizations seen in initial runs and reduce severity of minor losses seen in initial runs. **Table 5** Shows the furnace runs designed by DesignExpert 12 alongside the characterization results for the furnace sample boats. Furnace sample boats were characterized separately to determine the effect of gas flow on the synthesis process.

Table 5. Response surface scale-up furnace run parameters and synthesis results.

Furnace Run	Time	Temperature (°C)	Gas Type	Avg wt. % SiC Boat 1	Avg wt. % SiC Boat 2
1	4	1100	H_2	0	0
2	4	1400	Ar	5.67	5.67
3	6	1250	Ar	4.33	0
4	4	1400	H_2	3.33	15.33
5	8	1400	H_2	17.67	17.67
6	6	1250	Ar	2.33	0
7	4	1100	Ar	0.33	1
8	6	1250	Ar	12	0
9	8	1100	H_2	0	0
10	8	1100	Ar	0.2	0
11	8	1400	Ar	19	14.33
12	6	1250	H_2	3	4
13	6	1250	H_2	0	12.33
14	6	1250	H_2	3.33	13.67

Due to the high variance of the data points 12 and 14 listed in **Table 5**, they were removed from the analysis. These data points were found to be outside the normal range for the presented data and are thought to be inaccurate due to fluctuation in gas flow rate. It was found that if a high fluctuation in flow rate occurred then product was found to deposit inside the furnace tube or the gas exhaust tube skewing the data to show that these runs produced little to no SiC.

3.2.1. Boat 1

Table 6 shows the ANOVA analysis results for the silicon carbide wt. % characterized in Boat 1 samples, when compared to the furnace run parameters.

Table 6. ANOVA diagnostic data for scale-up runs, Boat 1.

Source	F-value	P-value
Model	130.96	0.<0.0001
A-Time	54.87	0.0001
B-Temperature	402.48	0.<0.0001
C-Gas type	4.90	0.8651

The ANOVA from Boat 1 was used to assess how well the model will fit the data and how statistically valid the model will be. The f-value in the second column shows that the model is significant, and the p-values associated with the model terms; A, B, and C show that these terms are significant to the model. This means that all these terms function to increase or decrease yield of silicon carbide when adjusted.

Fit statistics for the model, which indicate how accurate the model is likely to be, are shown in **Table 7.**

Table 7. ANOVA fit statistics for silicon carbide synthesis scale-up runs, Boat 1.

Std. Dev.	0.202	**R^2**	0.987
Mean	1.78	**Adjusted R^2**	0.980
Adeq Precision	32.6	**Predicted R^2**	0.970

The R^2 value shown in the table above is a measure of how well the terms in the model fit along a curve or a line while the adjusted R^2 takes into account how many data points are present, if data points that don't fit the model are included then the adjusted R^2 will stray from the R^2 value. In this data the R^2 and adjusted R^2 are in agreement meaning they have a difference value of less than 0.2 showing that the model does not include irrelevant variables.

Figure 9 (a) shows the normal plot of residuals for sample Boat 1 and shows the data points following the red line with minimal scatter while **Figure 9 (b**) shows the predicted value of synthesis content, as the black line, vs the actual measured value of silicon carbide in the samples.

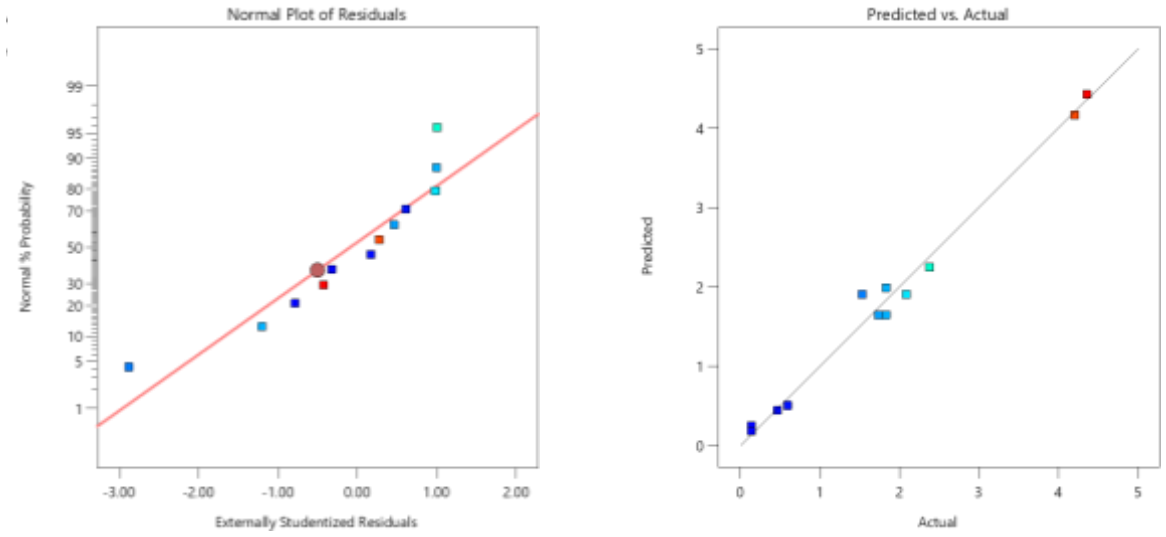

(a) **(b)**

Figure 9. Normal Plot of Residuals (left) and Predicted vs. Actual (right) diagnostics graph for scale-up runs analyzing Boat 1.

The data in the normal plot of residuals generally follows the line and does not produce an s shaped curve indicating that the use of a transform for the model is not needed. The predicted vs actual graph shows how well the model can predict response values and is used to determine if there are variable ranges the model cannot predict well. The data as presented by these graphs can be reasonably predicted by the model.

Figure 10 shows the residuals vs predicted graph and the Cook's used to determine if any further data transform is needed or if any data points may need to be removed.

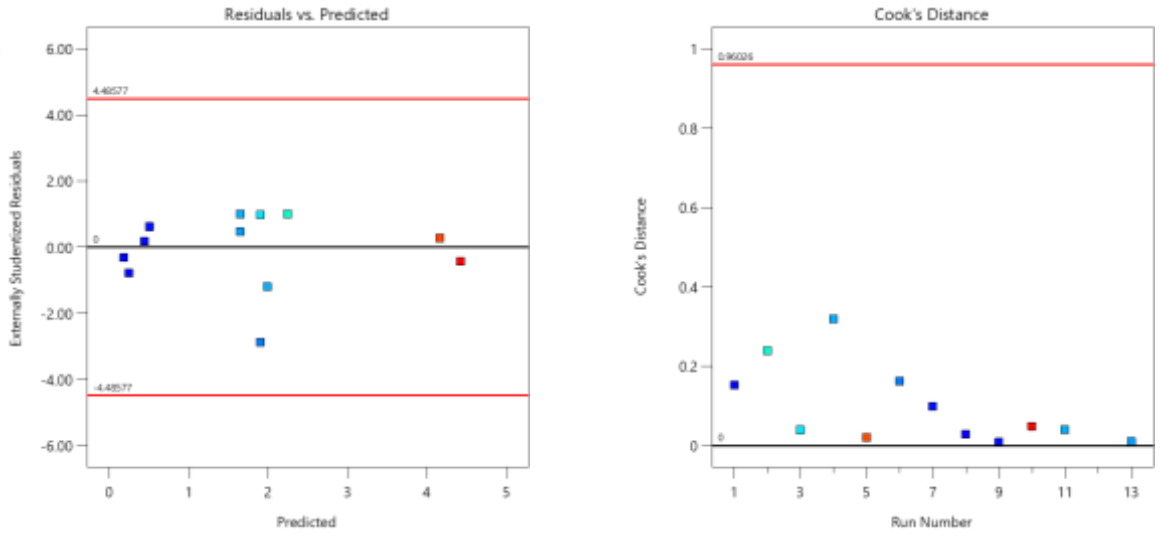

(a) **(b)**

Figure 10. a) Residuals vs. Predicted diagnostics graph for scale-up runs analyzing Boat 1 with a square root transform. b) Cook's distance graph for scale-up runs analyzing Boat 1 with a square root transform.

From the residuals vs the predicted values in

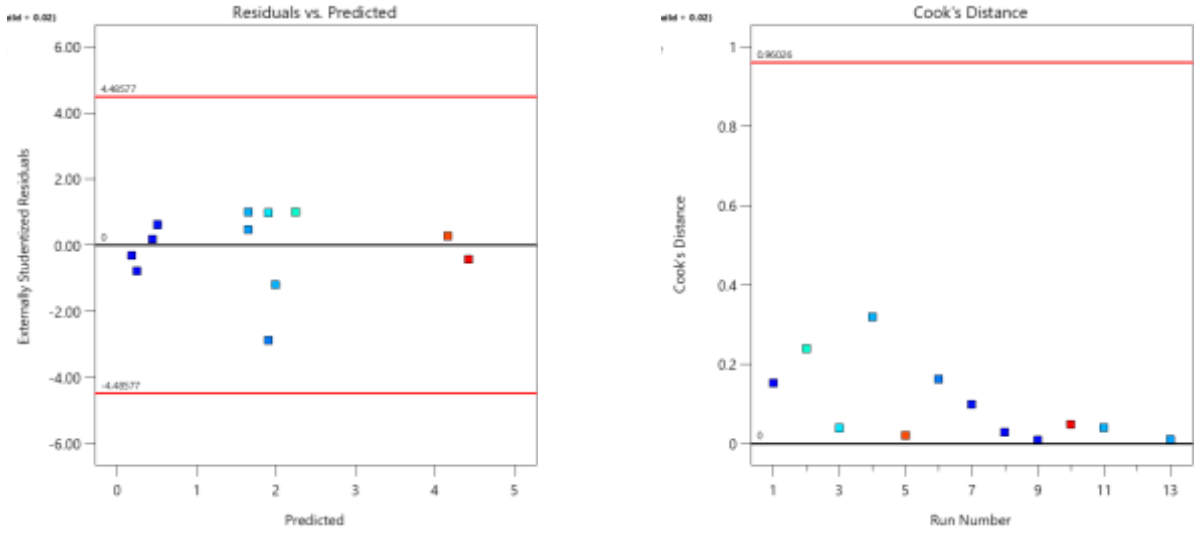

(a) **(b)**

Figure *10* (a), the graph shows a random scatter near the middle black line indicating that the square root transform is satisfactory, and that the data will be best modeled under the conditions chosen with the available data.

The Cook's distance is shown in **Figure 10 (b)** on the right-hand side. The cooks distance shows the sum off the difference values of the actual data when compared to the predicted data. Data points that fall close to zero are points that were accurately predicted by the model and points that have a higher Cook's distance are points that the model did not predict accurately. All points in this graph fall below the red line indicating no data points need to be removed.

Figure 11 shows the interaction graph linking the connection between silicon carbide yield and temperature for the system under Ar atmosphere. The red lines show the interaction the two variables have at 8 h while the black set of lines show the interaction at 4 h.

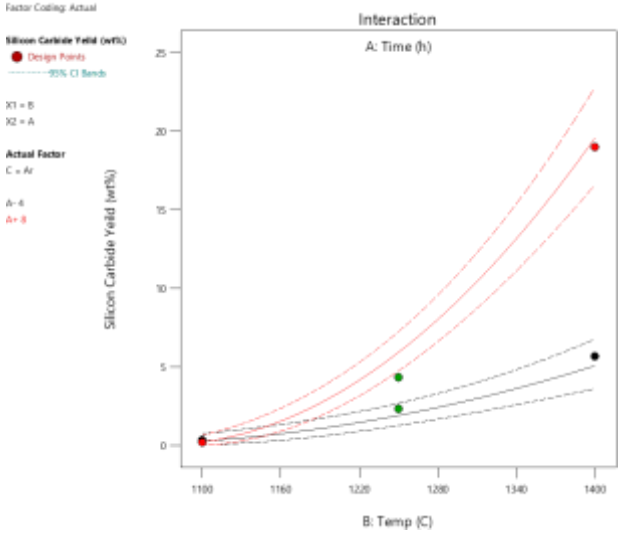

Figure 11. interaction graph showing the connection between time and temperature at 4h and 8h under Ar atmosphere.

This graph shows that at longer periods of time the higher the yield for silicon carbide and shows the time variable to be interconnected with temperature. The points on the graph show the upper, lower, and midpoints in the data. The upper and lower bounds fall within the confidence interval for the model, however one of the midpoints fall just outside in the 8 h interaction indicating some shortcomings with the model's ability to predict outcomes.

Figure 12 shows the interaction graph linking the connection between silicon carbide yield and temperature for the system under H_2 atmosphere. The red lines show the interaction the two variables have at 8h while the black set of lines show the interaction at 4 h.

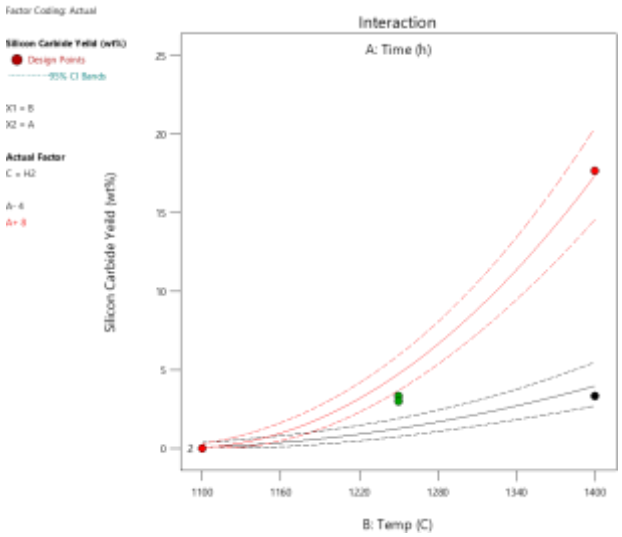

Figure 12. Interaction graph showing the connection between time and temperature at 4 h and 8 h under H_2 atmosphere.

Data points on the graph fall in between the dashed lines which is the confidence interval in the upper and lower areas while the midpoints fall outside of the confidence interval reflecting the need for more experimentation and tighter control over experimental parameters.

Figure 13 is the response surface for the silicon carbide synthesis samples in Boat 1 under argon gas.

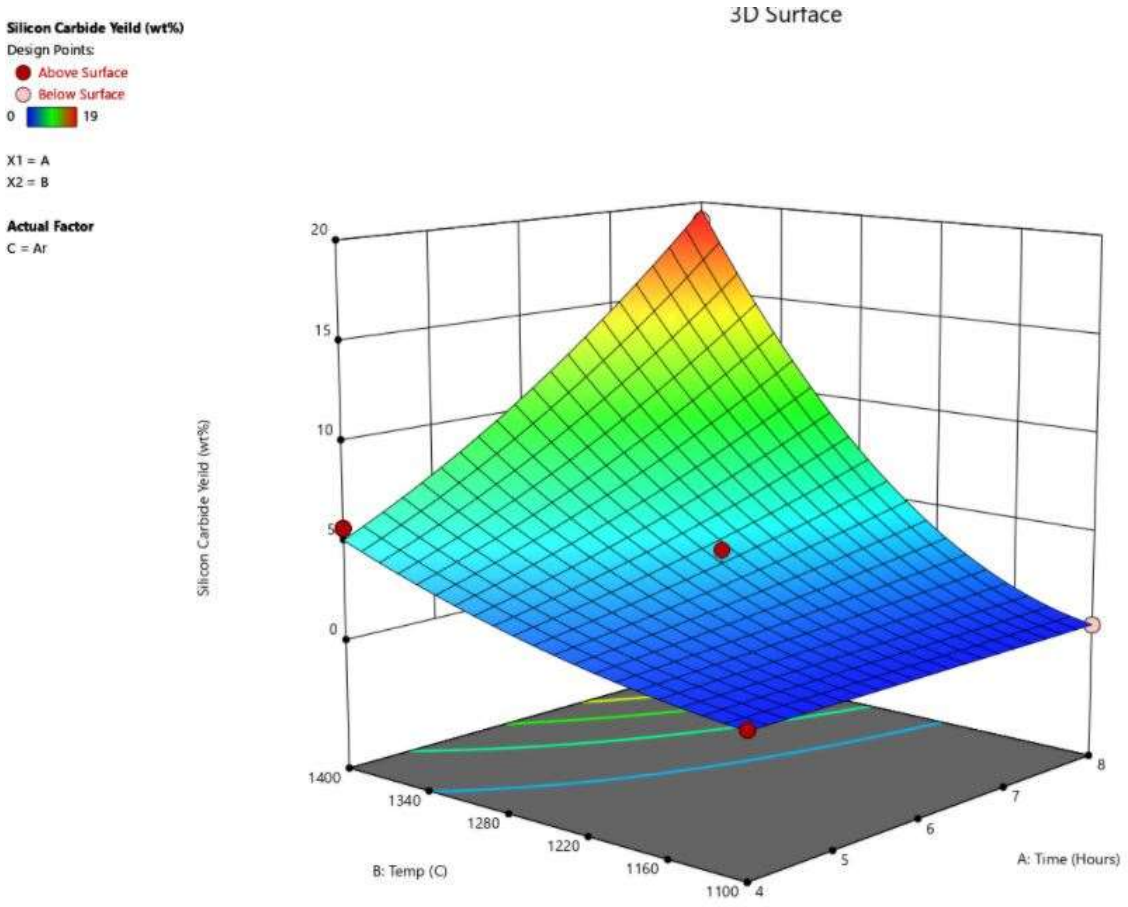

Figure 13. Silicon carbide synthesis response surface model of scale-up runs performed under argon, in boat one.

The model shows that a larger amount of silicon carbide is produced at temperatures above 1200 °C with the best yield temperature being 1400 °C, which was the upper bound chosen for this experiment. Longer furnace runs also increased the yield of silicon carbide however this was not as much of a limiting factor as shown by the graph, an 8 h run performed at 1100 °C to 1200 °C produced less silicon carbide than a 4 h run performed at 1400 °C indicating that the process is thermally driven.

Figure 14 is the response surface for the silicon carbide synthesis samples in Boat 1 under hydrogen gas.

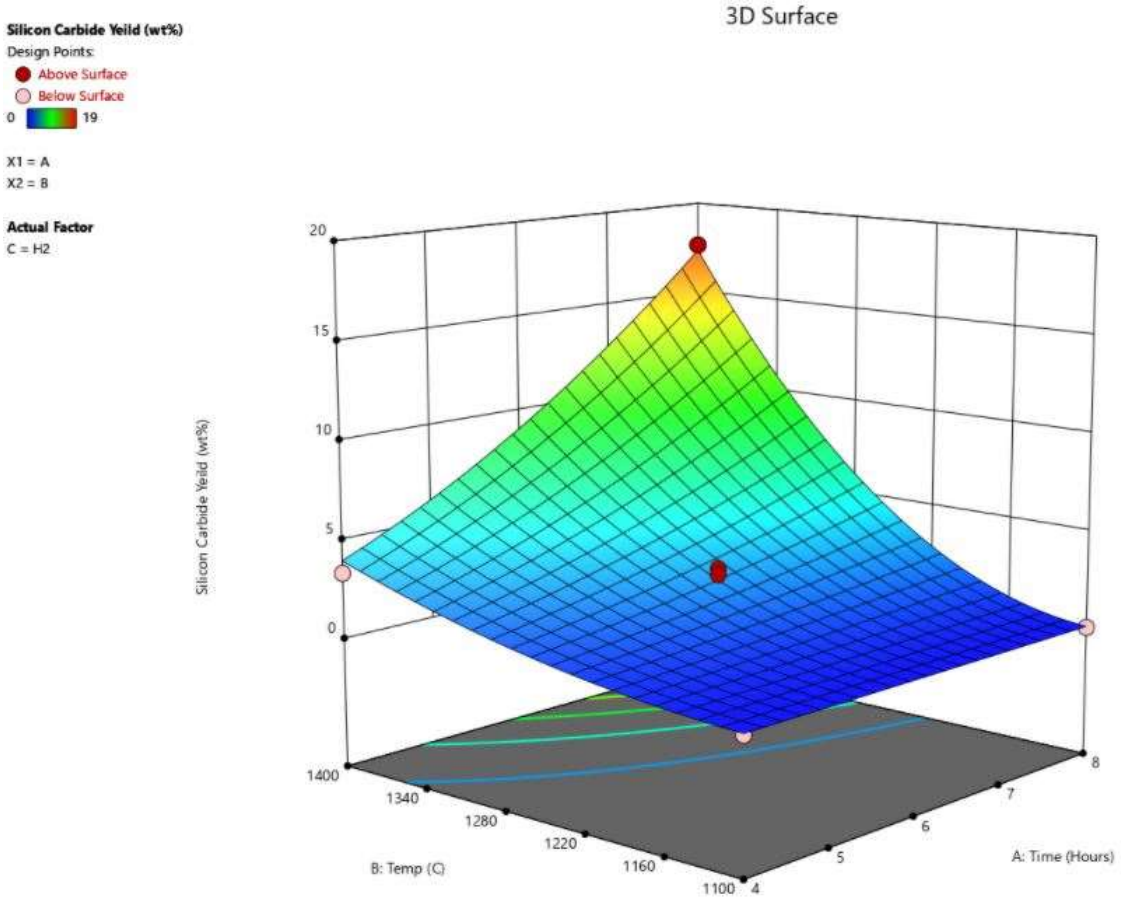

Figure 14. Silicon carbide synthesis response surface model of scale-up runs performed under hydrogen, in Boat 1.

The response surface for hydrogen also shows that a longer time and temperature will lead to higher silicon carbide yield, however when these two response surface graphs are compared with each other the gas composition does not have as much of an effect, with the hydrogen model showing less silicon carbide yield. This could be due to the affect time has on the model. The model shows that time spent in the furnace does not affect yield as much as temperature, and because the hydrogen only interacts with the sample when the furnace has come up to temperature, the chemical reaction may already be mostly completed by the time hydrogen is introduced.

3.2.2. Boat 2

Table 5 shows the SiC yield results for Boat 2. These results are unable to be modeled as they are not found to be representative of the system. Boat 2 was the first boat to come into contact with the gas stream flowing through the furnace, when the gas flow was too high, or was disrupted, it is thought that the gas intermediate phase of silicon oxide was blown to deposit onto the surface of Boat 1 or blown

out of the furnace. This supports the existence of a gas intermediate phase and shows the gas flow rate as a variable that needs to be further constrained or tested.

3.3. Sample Imaging

The SEM images were taken of a sample to determine the composition of the white material seen on its surface. This material when analyzed under the SEM was determined to be silicon carbide fibers ranging from 6-10 µm thick.

Samples taken out of the furnace are shown in **Figure 15** on the top, samples below the divider are precursor material.

Figure 15. images of samples before and after carburization. On the right is Boat 2 and on the left is Boat 1.

Gas flow occurs from right to left with material being most commonly deposited on Boat 1 seen in the image. This illustrates that the material was being carried from Boat 1 to Boat 2 and reacting to the carbon on the surface of the sample. Once the surface of the sample became crowded with SiC, SiO was no longer able to react with the carbon and SiO was blown out of the furnace instead.

Figure 16. shows a furnace run sample at 1200 °C for 6 h under Ar gas. These images were taken of the top part of the sample that had the most contact with the purge gas flow.

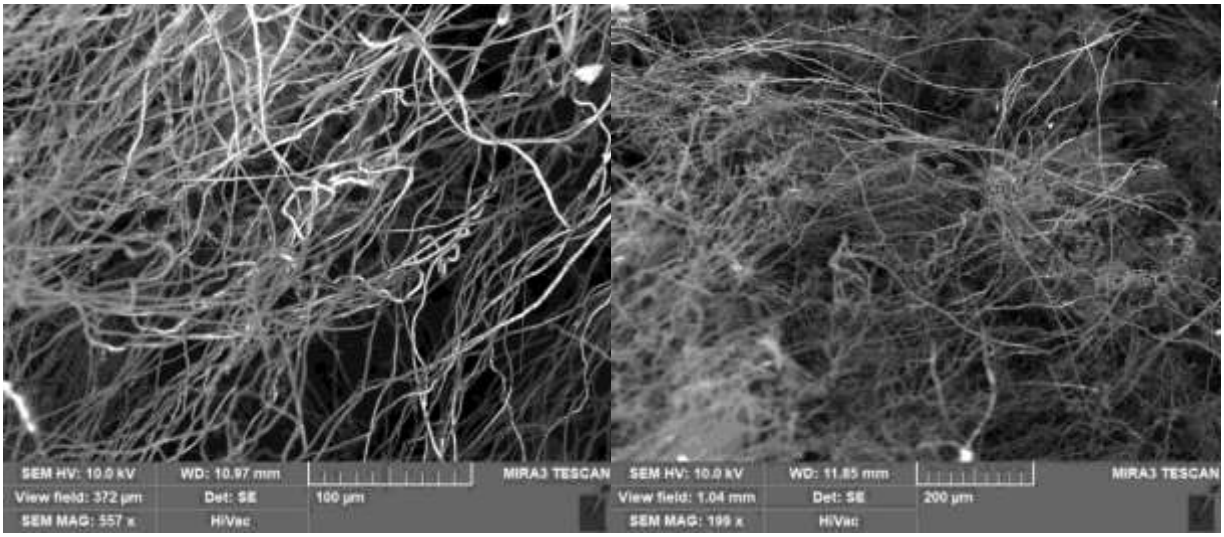

Figure 16. SEM images of silicon carbide fibers captured at different magnifications described in the figure.

The strands shown have a uneven texture indicative of silicon carbide whiskers growing due to a gas phase [20]. The strands were also found to be in line with the gas flow through the furnace, however fiber alignment characteristics was difficult to preserve when mounting on a sample stub for observation.

Figure 17. above shows a SEM image of the silicon carbide formations found on the top of the carburized sample. These images depict strands of silicon carbide grown on the left and what appears to be nucleation sites for these strand growths on the right.

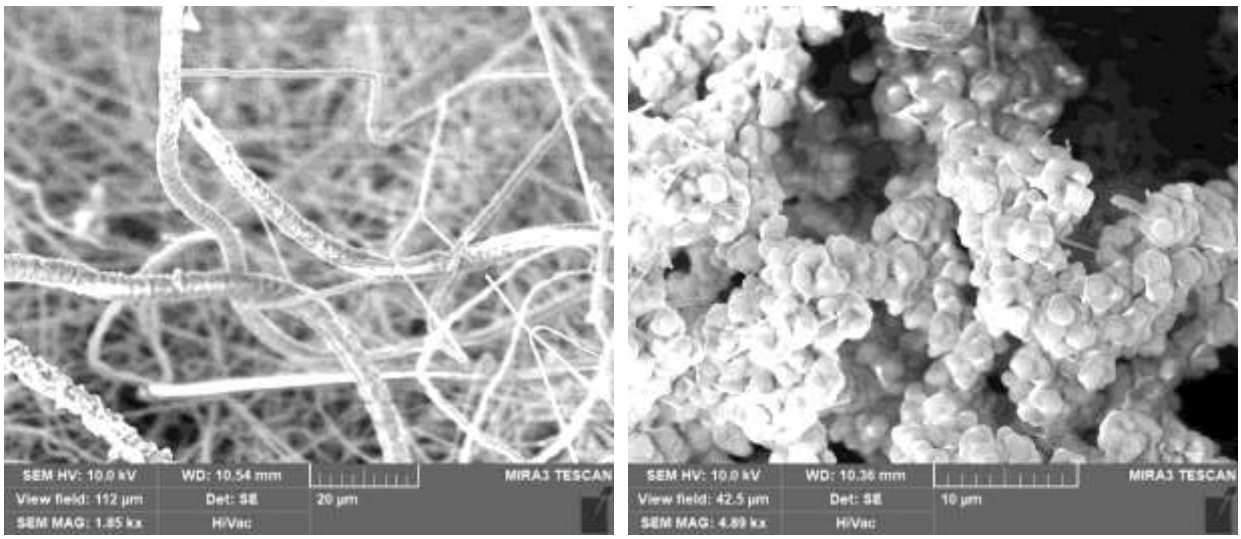

(a) (b)

Figure 17. (a) SEM images of silicon carbide fibers and (b) a cluster of silicon carbide nucleation growth sites.

Another indication in favor of a gas intermediate phase being involved was that layers of white particles of what is assumed to be silicon carbide, found in the furnace tube itself and the gas outlet tube connected to the bubbler before the gas was discharged. On several failed runs, gas flow was mistakenly or accidently set at a higher flow rate than 0.5 L/min, for either H_2 or Ar, resulting in little to no visible

product indicated by a white outer layer found on the sample boat. This layer of material found in the discharge tube and on the furnace was unable to be characterized however due to the small amount present. Additionally, risk of contamination from material from prior experiments in the discharge tube and bubbler was too high to use material found in the tube and bubbler. These factors limit the effectiveness of the SiC capture method and is therefore assumed that some amount of product was lost to the furnace system and it is unclear what the true synthesis values are.

Due to the variation in gas flow resulting in little or no sample and the observations of the growths on top of the sample it is assumed that a lack of strict control over the gas flow rate has introduced error in the ability to fit the synthesis data to the created model and work done in the future would need to strictly control the gas flow rate and ensure that a collection system is implemented to ensure synthesis data can be collected.

5. Conclusions

The purpose of this study was to determine if it was possible to create silicon carbide reliably using the adsorption method outlined by previous studies. Silicon carbide nanofibers were created using this method and carburization behavior was modeled using Design expert 12. The models created showed a higher yield when temperatures were above 1250 °C and that temperature had a positive correlation with time. Gas composition was shown not to have as great an effect on yield, however with previous literature stating that H_2 improves SiC creation, it is possible that with stricter gas flow rate, higher yield could be achieved.

The gas flow rate is likely to be a significant variable as indicated by sample composition on the micro and macro level. Macro level samples were shown to have an outer layer of silicon carbide growth over the sample plane that encounters the gas flow. Once this layer was observed under SEM a more defined whisker structure was observed in the direction of the gas flow. These physical observations, combined with the lack of sample obtained at higher flow rates, indicate that an intermediate gas phase is likely present, and that flow rate is a variable that needs to be explored in future work.

4. Future work

Creating silicon carbide with the activated carbon adsorption method in the future should include stricter control of gas flow rate. This project showed that the silicon carbide fibers grew in the direction of gas flow, and most of the product was found on the top of the samples, indicating the need to test this parameter and determine its effect on fiber structure and its influence on the synthesis process. The gas intermediate phase should also be taken into consideration when attempting to recover or stop the loss of material that ends up on the inside of the exhaust tube or the inside of the furnace tube. To mitigate loss of material one recommendation would be to recirculate off gases coming from the furnace or to use $SiO_{(g)}$ in place of an inert gas.

The next step for this material would be the separation of the silicon carbide fibers from the excess activated carbon present. Due to the formation of material, it is possible that the whiskers could be mechanically removed from a majority of the carbon before further refinement however maintaining fiber structure after this initial removal will be an issue.

5. Acknowledgements

Research was sponsored by the Combat Capabilities Development Command Army Research Laboratory and was accomplished under Cooperative Agreement Number W911NF-15-2-0020. The views and conclusions contained in this document are those of the authors and should not be interpreted as representing the official policies, either expressed or implied, of the Combat Capabilities Development Command Army Research Laboratory or the U.S. Government. The U.S. Government is authorized to reproduce and distribute reprints for Government purposes notwithstanding any copyright notation herein.

6. References

[1] "Silicon carbide | chemical compound | Britannica.com." [Online]. Available: https://www.britannica.com/science/silicon-carbide. [Accessed: 19-Oct-2019].

[2] "Carbides | Introduction to Chemistry." [Online]. Available: https://courses.lumenlearning.com/introchem/chapter/carbides/. [Accessed: 25-Oct-2019].

[3] G. S. Upadhyaya *et al.*, *Cemented Tungsten Carbides Production, Properties and Testing*, 1st ed., vol. 1, no. 30 V. 1998.

[4] "Carbide | chemical compound | Britannica." [Online]. Available: https://www.britannica.com/science/carbide. [Accessed: 28-Apr-2021].

[5] G. C. Wallace, J. P. Downey, J. Chorney, K. Schumacher, and A. Mallard, "Synthesis of nanocrystalline carbide ceramics via reduction of anion-loaded activated carbon precursors," in *Minerals, Metals and Materials Series*, 2018, vol. Part F10, pp. 125–134.

[6] "Carbide Ceramics - Fraunhofer IKTS." [Online]. Available: https://www.ikts.fraunhofer.de/en/departments/structural_ceramics/nonoxide_ceramics/carbide_ceramics.html. [Accessed: 24-Mar-2020].

[7] T. Tiegs, "SiC Whisker Reinforced Alumina," in *Handbook of Ceramic Composites*, Springer US, 2006, pp. 307–323.

[8] "SiC Properties | Washington Mills." [Online]. Available: https://www.washingtonmills.com/silicon-carbide/sic-properties. [Accessed: 29-Apr-2021].

[9] "Silicon Carbide SiC Material Properties." [Online]. Available: https://accuratus.com/silicar.html. [Accessed: 30-Apr-2021].

[10] "Ramsdell Notation for SiC Polytypes." [Online]. Available: https://www.tf.uni-kiel.de/matwis/amat/semi_en/kap_a/basics/ba_1_1.html. [Accessed: 19-Oct-2019].

[11] "3.3.2 Bravaisgitter und dichteste Kugelpackung." [Online]. Available: https://www.tf.uni-kiel.de/matwis/amat/mw1_ge/kap_3/backbone/r3_3_2.html. [Accessed: 19-Oct-2019].

[12] "10.1.1 Siliconcarbide - Materials Aspects." [Online]. Available: https://www.tf.uni-kiel.de/matwis/amat/semi_en/kap_a/backbone/ra_1_1.html. [Accessed: 19-Oct-2019].

[13] H. N. Baumann, "The Relationship of Alpha and Beta Silicon Carbide."

[14] T. S. Aarnæs, E. Ringdalen, and M. Tangstad, "Silicon carbide formation from methane and silicon monoxide," *Sci. Rep.*, vol. 10, no. 1, pp. 1–11, Dec. 2020.

[15] X. Li, G. Zhang, O. Ostrovski, and R. Tronstad, "Effect of gas atmosphere on the formation of silicon by reaction of SiC and SiO2," *J. Mater. Sci.*, vol. 51, no. 2, pp. 876–884, Jan. 2016.

[16] H. J. Hwang, K.-J. Lee, Y.-T. An, B.-H. Choi, and W.-S. Seo, "Synthesis of-silicon carbide nanofiber from an exfoliated graphite and amorphous silica," *Mater. Chem. Phys.*, vol. 134, pp. 13–15, 2012.

[17] T. Kimoto and J. A. Cooper, *Fundamentals of Silicon Carbide Technology: Growth, Characterization, Devices and Applications*, vol. 9781118313527. Wiley-IEEE Press, 2014.

[18] K. R. Karasek, S. A. Bradley, J. T. Donner, H. C. Yeh, and J. L. Schienle, “Characterization of recent silicon carbide whiskers,” *J. Mater. Sci.*, vol. 26, no. 1, pp. 103–111, Jan. 1991.

[19] L. Wang, H. Wada, and L. F. Allard, “Synthesis and characterization of SiC whiskers,” *J. Mater. Res.*, vol. 7, no. 1, pp. 148–163, 1992.

[20] S. R. NUTT, “Defects in Silicon Carbide Whiskers,” *J. Am. Ceram. Soc.*, vol. 67, no. 6, pp. 428–431, 1984.

[21] H. Wang, Y. Berta, and G. S. Fischman, “Microstructure of Silicon Carbide Whiskers Synthesized by Carbothermal Reduction of Silicon Nitride,” *J. Am. Ceram. Soc.*, vol. 75, no. 5, pp. 1080–1084, 1992.

[22] V. Raman, G. Bhatia, A. K. Mishra, S. Bhardwaj, and K. N. Sood, “Synthesis of silicon carbide nanofibers from pitch blended with sol-gel derived silica,” *Mater. Lett.*, vol. 60, no. 29–30, pp. 3906–3911, Dec. 2006.

[23] K. Vyshnyakova, G. Yushin, L. Pereselentseva, and Y. Gogotsi, “Formation of porous SiC ceramics by pyrolysis of wood impregnated with silica,” *Int. J. Appl. Ceram. Technol.*, vol. 3, no. 6, pp. 485–490, Nov. 2006.

[24] Ö. Çeçen, Ferhan, Aktaş, *Activated Carbon for Water and Wastewater Treatment: Integration of Adsorption and Biological Treatment*. Wiley-VCH Verlag GmbH & Co. KGaA, 2012.

[25] H. F. Wertheim *et al.*, “Studying the effectiveness of activated carbon R95 respirators in reducing the inhalation of combustion by-products in Hanoi, Vietnam: A demonstration study,” *Environ. Heal. A Glob. Access Sci. Source*, vol. 11, no. 1, 2012.

[26] N. W. E. Contributors, “Activated carbon,” *New World Encyclopedia, .*, 2019. [Online]. Available: www.newworldencyclopedia.org/p/index.php?title=Activated_carbon&oldid=1026779. [Accessed: 18-Mar-2020].

[27] R. W. Derlet and T. E. Albertson, “Cl iniclt Review Activated Charcoal-Past, Present and Future.”

[28] S. Bubanale and M. Shivashankar, “History, Method of Production, Structure and Applications of Activated Carbon.”

[29] F. R. R. Harry Marsh, *Activated Carbon*, 1st ed. Elsevier Science, 2006.

[30] Elizabeth Raiha, “B3R65H-Location1-656x,” Butte.

[31] G. Wallace, “Synthesis of Carbide Ceramics Via Reduction and Carburization of Oxyanions aAdsorbed onto an Activated Carbon Matrix,” 2020.